A composite rupture model for the great 1950 Assam earthquake across the cusp of the East Himalayan Syntaxis

A. Coudurier-Curveur, P. Tapponnier, E. Okal, J. van Der Woerd, E. Kali, S. Choudhury, S. Baruah, M. Etchebes, Ç. Karakaş

Earth and Planetary Science Letters 531 (2020) 115928

Contents lists available at ScienceDirect

Earth and Planetary Science Letters

www.elsevier.com/locate/epsl

A composite rupture model for the great 1950 Assam earthquake across the cusp of the East Himalayan Syntaxis

A. Coudurier-Curveur [a,*], P. Tapponnier [b], E. Okal [c], J. Van der Woerd [d], E. Kali [d], S. Choudhury [e], S. Baruah [f], M. Etchebes [g], Ç. Karakaş [a]

[a] Earth Observatory of Singapore, Nanyang Technological University, 50 Nanyang Avenue, Singapore 639798, Singapore
[b] Institute of Crustal Dynamics, China Earthquake Administration, Haidian, Beijing, 100085, China
[c] Department of Earth and Planetary Sciences, Northwestern University, Evanston, IL 60208, United States
[d] Institut de Physique du Globe de Strasbourg, UMR 7516 CNRS, Université de Strasbourg, 5 rue Descartes, 67084 Strasbourg cedex, France
[e] Wadia Institute of Himalayan Geology, Dehradun-248 001, Uttarakhand, India
[f] CSIR-North-East Institute of Science and Technology, Jorhat-785 006, Assam, India
[g] Schlumberger-Doll Research Center, Cambridge, MA 02139-1578, USA

ARTICLE INFO

Article history:
Received 18 June 2019
Received in revised form 23 October 2019
Accepted 26 October 2019
Available online 15 November 2019
Editor: J.P. Avouac

Keywords:
Assam
Himalayan earthquakes
tectonic geomorphology
relocated aftershocks
landslide distribution
surface rupture

ABSTRACT

Although the $M_w = 8.7$, 1950 Assam earthquake endures as the largest continental earthquake ever recorded, its exact source and mechanism remain contentious. In this paper, we jointly analyze the spatial distributions of reappraised aftershocks and landslides, and provide new field evidence for its hitherto unknown surface rupture extent along the Mishmi and Abor Hills. Within both mountain fronts, relocated aftershocks and fresh landslide scars spread over an area of ≈330 km by 100 km. The former are more abundant in the Abor Hills while the later mostly affect the front of the Mishmi Hills. We found steep seismic scarps cutting across fluvial deposits and bounding recently uplifted terraces, some of which less than two thousand years or even a couple centuries old, at several sites along both mountain fronts. They likely attest to a minimum 200 km-long 1950 surface rupture on both the Mishmi and Main Himalayan Frontal Thrusts (MT and MFT, respectively), crossing the East Himalayan Syntaxis. At two key sites (Wakro and Pasighat), co-seismic surface throw appears to have been over twice as large on the MT as on the MFT (7.6 ± 0.2 m vs. $>2.6 \pm 0.1$ m), in keeping with the relative, average mountain heights (3200 m vs. 1400 m), mapped landslide scar numbers (182 vs. 96), and average thrust dips (25–28° vs. 13–15°) consistent with relocated aftershocks depths. Corresponding average slip amounts at depth would have been ≈17 and ≈11 m on the MT and MFT, respectively, while surface slip at Wakro might have reached ≈34 m. Note that this amount of superficial slip would be out of reach using classic paleo-seismological trenching to reconstruct paleo-earthquake history. Most of the 1950 first arrivals fit with a composite focal mechanism co-involving the two shallow-dipping thrust planes. Their intersection lies roughly beneath the Dibang Valley, implying forced slip parallel to GPS vectors across the East Himalayan Syntaxis. Successive, near-identical, terrace uplifts at Wakro suggest near-characteristic slip during the last two surface rupturing earthquakes, while terrace boulder ages may be taken to imply bi-millennial return time for 1950-size events. As in Nepal, East-Himalayan mega-quakes are not blind and release most of the elastic, interseismic shortening that accumulates across the range.

1. Introduction

Great ($M_w > 8$) 19th/20th century Himalayan earthquakes were long considered blind, which made research on their exact sources and return times difficult (e.g., Yeats et al., 1992; Nakata, 1989; Ader et al., 2012). The Assam earthquake of 15 August 1950 (also known as Chayu or Medog earthquake), the largest continental event ever recorded instrumentally ($M_w \approx 8.6$–8.7) (Ben-Menahem et al., 1974; Chen and Molnar, 1977), has been no exception to that belief. Characterization of its source and focal mechanism, and therefore identification of the fault plane(s) involved in the rupture, are still a matter of controversy. While its epicenter was located in remote mountain terrain, northeast of the Mishmi Hills (Kingdon-Ward, 1951, 1953a, 1953b), above the Mishmi Thrust (MT) and close to the Po-Qu-Lohit strike-slip fault (Fig. 1 and Table 1), most of the aftershocks spread over several hundred

* Corresponding author at: Institut de Physique du Globe de Paris, 75238 Paris, France.
E-mail address: acoudurierc@ntu.edu.sg (A. Coudurier-Curveur).

https://doi.org/10.1016/j.epsl.2019.115928

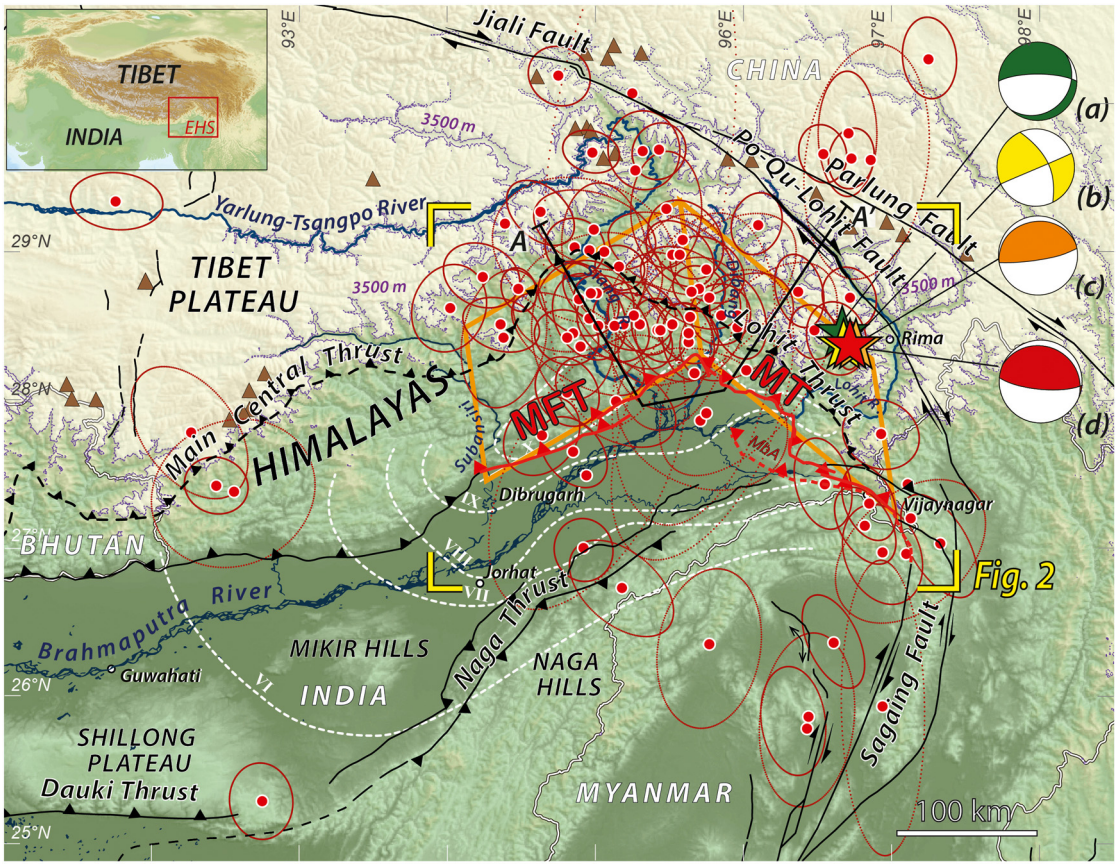

Fig. 1. Active faulting around East Himalayan Syntaxis (EHS) (updated from Tapponnier and Molnar, 1977; Armijo et al., 1989) superimposed on colored SRTM 3 DEM (large-scale location: red rectangle, in top-left inset). Surface traces of the great, 15/8/1950, Assam earthquake rupture on Main Himalayan Frontal Thrust (MFT) and Mishmi Thrust (MT) are outlined in red (dashed where inferred along Manabhum anticline front (MbA; Fig. 2). Older, Main Central and Lohit Thrusts traces are also shown (dashed black). Colored stars and beach-balls are 1950 mainshock epicenter locations and focal mechanisms from different sources (Green: (a) Tandon, 1955; Yellow: (b) Ben-Menahem et al., 1974, Herrin et al., 1962; Orange: (c) Chen and Molnar, 1977; Red: (d) this study) (see coordinates in Table 1). Red dots with error ellipses are our relocations of aftershocks in first four months after 1950 mainshock. Orange parallelograms are projections of inferred co-seismic fault planes containing the mainshock epicenters, the majority of aftershocks, and most mapped landslide scars (Fig. 2). Isoseismal lines (dashed white) are from Poddar (1950) (Mercalli scale, modified from Rossi-Forel). Brown triangles highlight Himalayan summits with elevations above 6000 m. Thin, purple, 3500 m contour line separates Tibet plateau (light yellow) and Abor Himalayas and Mishmi ranges (green) (e.g., Avouac, 2003; Bollinger et al., 2004). Brahmaputra drainage system is in blue. Composite A–A′ line refers to combined cross-sections in Fig. 3. (For interpretation of the colors in the figure(s), the reader is referred to the web version of this article.)

Table 1
List of focal mechanisms, moment estimates, magnitudes, and epicentral locations of 1950 Assam earthquake, from different published sources.

Reference	Focal mechanism				Seismic moment		Conventional magnitudes		Coordinates (WGS84, Dec. Deg.)	
	Φ (°)	δ (°)	λ (°)	Nature	10^{21} (N·m)	M_w	Value	Scale	Lat.	Long.
Gutenberg and Richter (1954)							8.6	PAS (M_s)		
Abe (1981)							8.6	M_s		
Tandon (1955)	270	75	285	Normal faulting					28.46N	96.67E
Ben-Menahem et al. (1974)	334	60	175	Strike-slip	21	8.8			28.38N	96.68E
Chen and Molnar (1977)	260	12	90	Thrust	9.5	8.6			28.38N	96.76E
Okal (1992)					14	8.7				
This study	293	16	107	Composite	13	8.7			28.38N	96.72E

kilometers within the Abor Hills, highlighting a possible source on the Main Himalayan Frontal Thrust (MFT). Likewise, as derived by different authors from first motion datasets and spectral amplitudes, the mainshock focal mechanism remained controversial, implying either normal, thrust, or oblique strike-slip faulting, or possibly a combination of the latter two (Tandon, 1955; Ben-Menahem et al., 1974; Chen and Molnar, 1977; Molnar and Deng, 1984) (Fig. 1 and Table 1). Also, while widespread liquefaction (e.g., Reddy et al., 2009; Rajendran and Rajendran, 2011), large landslides, and catastrophic debris flows were widely described in the Assam plain (Tandon, 1950; Kingdon-Ward, 1953a, 1953b; Ramachandra Rao, 1953), and despite dedicated research (e.g., Kumar et al., 2010; Jayangondaperumal et al., 2011), no unequivocal evidence of a primary surface rupture was found for a long time. Recently, however, in Pasighat, ≈400 m northeast of one roadside site previously identified to bear clear trace of 1950 surface deformation (Figs. 2 and 6b; Kali et al., 2013; Coudurier Curveur et al., 2014a, 2014b), shallow (≈2 m) trenching has locally confirmed the existence of near-surface faulting in the mid-20th century, hence likely in 1950 (Priyanka et al., 2017).

Following the discovery of a clear rupture for the great 1934 ($M \approx 8.4$) earthquake in Nepal (Sapkota et al., 2013; Bollinger et al., 2014) as well as evidence for medieval surface ruptures of large magnitude events in the Western Himalaya (e.g., 1300–1400 A.D., Kumar et al., 2001; Malik et al., 2008), we systematically revisited the whole extent of the Arunachal Pradesh mountain front to

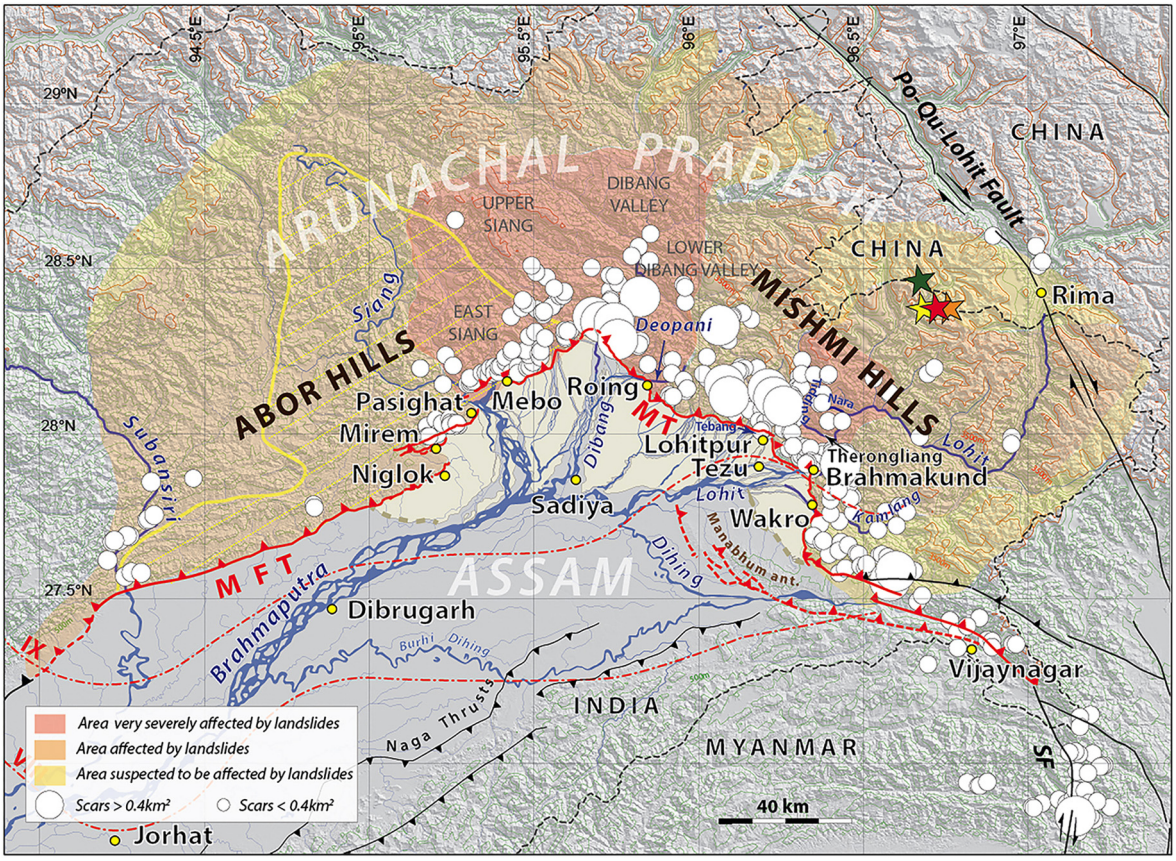

Fig. 2. 1950 landslides and debris flows. 1950 inferred earthquake surface rupture (Fig. 1) is outlined in red. Mainshock epicentral locations, as in Fig. 1. White circles correspond to 451 picks of landslides scars, from detailed interpretation of Google Earth images (Large circles for landslide scars areas between 0.4 km^2 and 4 km^2; Table S1). Areas of Arunachal Pradesh plain devastated by debris flow deposits (south of MFT and MT) are outlined in beige. Pale red, orange, and yellow zones are mountain areas with different degrees of slope devastation, from post-event aerial survey (Ramachandra Rao, 1953; Ben-Menahem et al., 1974). Yellow contour delimits the Siang window. Isoseismal lines VIII and IX (dashed red) are from Poddar (1950) (Mercalli scale, modified from Rossi-Forel). 500 m topographic contours are from CARTOSAT DEM. SF: Sagaing Fault. Yellow dots are place names in Figs. 3 and 4.

search for evidence of a recent emergent break, assess the existence of previous ones, and determine their geometry and length. Because the 1950 mesoseismal area is densely forested, the field identification of active/young fault scarps and of steep terrace risers incised by permanent rivers is challenging, which may account for the scarcity of previous neotectonic studies. Across a few accessible scarps, we used topographic leveling measurements to separate recent, potentially 1950 co-seismic offsets from older cumulative offsets. Our field observations and measurements of surface deformation along both the Mishmi and Abor Hills mountain fronts were then combined with our reappraisal of the aftershocks and triggered landslide scars distributions to discuss an earthquake source model consistent with first-order, large-scale topographic and geodetic evidence.

2. Mesoseismal surface effects and aftershock distribution of the 1950 Assam earthquake

The most spectacular effect of the 1950 Assam earthquake was the devastation of the Mishmi and Abor hills slopes and foreland by catastrophic landslides and associated debris flows (Kingdon-Ward, 1951; Ramachandra Rao, 1953) (Notes S1a, S2, Appendix A0, Fig. 2). An aerial survey carried out shortly after the earthquake revealed the extent of damage in both hillslopes (Ramachandra Rao, 1953; Ben-Menahem et al., 1974), summarized in the qualitative map of Fig. 2 (red, orange, and yellow regions). Two distinct, "very severely" affected zones are apparent on either side of the East Himalayan Syntaxis cusp (East Siang-Upper Siang-Dibang Valleys and Lower Lohit Valley, Fig. 2). Since large landslides can persist long after a causative earthquake (Note S1b, Nilsen and Brabb, 1975; Keefer, 1994; Meunier et al., 2007), as emphasized by the lack of significant changes in landslide scars location over the last 35 yr (Appendix A0 and Fig. S0), we mapped the present-day distribution and size of fresh landslide scars using recent satellite images (2006–2012) to further constrain the source parameters. Although such first-order mapping is not exhaustive, especially for the smallest landslides and in areas with mist or clouds, the landslide distribution shown in Fig. 2 (cf. Table S1) nevertheless fits well with the "very severely" affected areas mapped shortly after the earthquake. Note that, while most large landslide scars are located within the areas of maximum slopes (≈30–50°, Fig. S1a) and present-day rainfall (≈4–7 m/yr, Fig. S1b), they mostly and closely follow the Abor and Mishmi range-fronts (up to ≈80%, over a length of ≈400 km), while the maximum slope and rainfall areas extend much farther and elsewhere into the mountains.

If indicative of the extent of seismic rupture, the fresh scars mapped continuously along the Mishmi front all the way to the Myanmar border (≈96.5°E, Figs. 1 and 2) suggest that faulting in 1950 may have extended along the MT to the northernmost Sagaing Fault's main branch. The gap between these fresh scars and others farther south along that north-trending fault may suggest that faulting in 1950 stopped at the 50° bend between the two faults. The southernmost landslides might then be related to an earlier sequence of three M 7 to 7.6 events on the Sagaing strike-slip fault between 1906 and 1931. This would be consistent

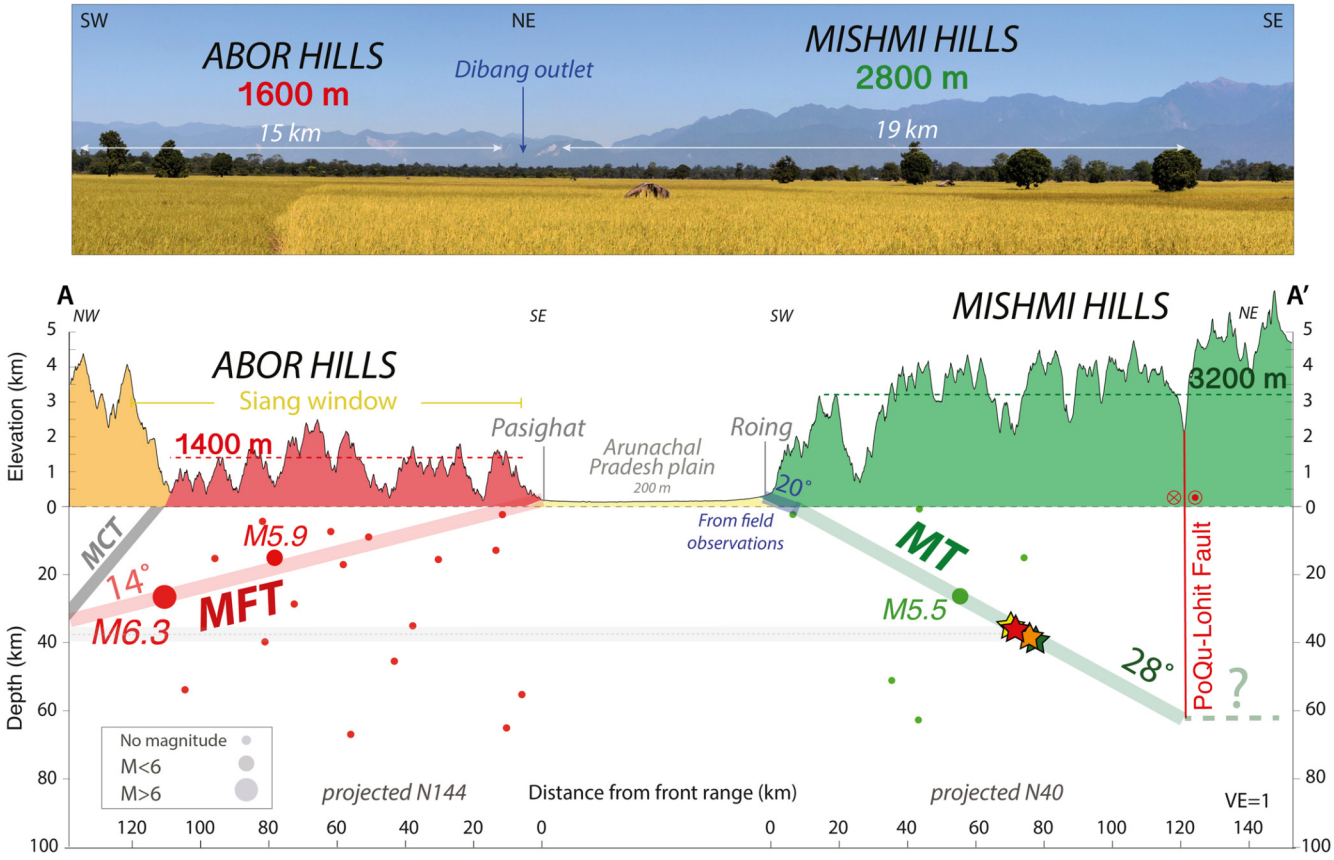

Fig. 3. Topography and tectonics of East Himalayan Syntaxis. (Top) North-looking view of sharp topographic drop between Mishmi Hills (east) and Abor Hills (west) at Dibang river outlet. Note remarkably flat, average range tops. (Bottom) Crustal sections of Abor/Mishmi syntaxis along combined A and A′ profiles (Fig. 1). Projected depths of 25 relocated aftershocks beneath Abor and Mishmi Hills are shown by red and green dots, respectively. The dips of MFT and MT thrusts (red and green lines, respectively) are consistent with the surface breaks locations and dips (Fig. 4), the average elevations of the corresponding frontal ranges (≈1400 m, red, and ≈3200 m, green, respectively), and the aftershock depths. Colored stars (as in Fig. 1) are projected locations of 1950 mainshock hypocenters. Note that the thrust geometries are likely more complex than simply planar. Main Central Thrust (MCT) "plane" location and dip are also indicated (dashed grey line). Vertical exaggeration (VE) of topography is 5.

with the outer limit of the area of "suspected" 1950 landslides (Fig. 2), if it was not just drown to follow the Myanmar border. Hence, we infer that faulting in 1950 stopped near Vijaynagar (27.19°N, 96.99°E) (Figs. 1 and 2). Similarly in the Abor Hills, clustered landslides along the Subansiri valley, near the outer limit of the "area affected by landslides" (Fig. 2), likely mark the western extent of faulting, close to the isoseismal line IX, implying that faulting on the MFT extended to ≈94°E in 1950. Furthermore, as observed for other large continental thrust earthquakes (e.g., 2008, $M_w = 7.9$, Wenchuan event), we interpret the dense distribution of the largest landslide scars along the Mishmi front to attest to particularly large peak accelerations, in turn possibly linked with particularly large co-seismic displacements on the MT (Fig. 2) (e.g., Meunier et al., 2007; Yuan et al., 2013).

Given the lack of observed surface faulting at the time, inferences on faulting and initial source length estimates relied only on the initial aftershock distribution (Kanamori and Allen, 1986). A 250 km-long source was first inferred using the spatial distribution of 54 relocated aftershocks recorded in the first 8 months after the mainshock (e.g., Tandon, 1954; Ben-Menahem et al., 1974; Chen and Molnar, 1977). Since the difference between source length and aftershock zone extent is commonly small for large earthquakes (e.g., dePolo and Slemmons, 1990; Wells and Coppersmith, 1994), we re-evaluated the distribution of the aftershocks using all 94 events listed by the International Seismological Summary (ISS) for the 4 months following the earthquake. We relocated them using the iterative interactive method of Wysession et al. (1991) (Fig. 1, Table S2, Note S3). The depths of 46 of these hypocenters could be retrieved by the floating depth relocation approach developed by Rees and Okal (1987) (Table S3). We verified that the distance between fixed and floated epicenters did not exceed a few kilometers.

At a regional scale, aside from a few distant (likely triggered) events along the Cona/Yarlung-Zangbo graben, across the Naga Hills, north of the Po-Qu fault, and along the northwestern Sagaing fault (Fig. 1), most of the aftershocks, within their confidence ellipses, lie beneath the Abor and Mishmi ranges. They are mostly located west of the relocated mainshock epicenters, all four of which are consistent with a deep rupture nucleation just west of the Po-Qu-Lohit fault (Fig. 1). They extend over a length of ≈350 km between the northernmost extremity of the Sagaing Fault main branch near Vijaynagar to the east, and the Subansiri River to the west (Fig. 1). The principal aftershock zone is bounded southwards by the Main Himalayan Frontal Thrust (MFT) and Mishmi Thrust (MT) faults, and to the northwest and northeast by the High Himalayan range and Po-Qu–Lohit strike-slip fault, respectively. Both the epicenter locations and the aftershock distribution imply coupled co-seismic slip on both the MT and MFT, possibly down to these geological boundaries (Figs. 1 and 3). Note that the smaller number of aftershocks in the Mishmi Hills may be suggestive of more complete stress release on the MT during the mainshock. Among the 46 hypocenter depths we retrieved, we used the 25 foci located beneath the Abor and Mishmi Hills to infer plausible, planar geometries for the MFT and MT in cross-section. Such selected data suggest that the MT may be about twice as steep as the MFT, with dip angles of ≈28° and ≈14°, respectively, in keeping with

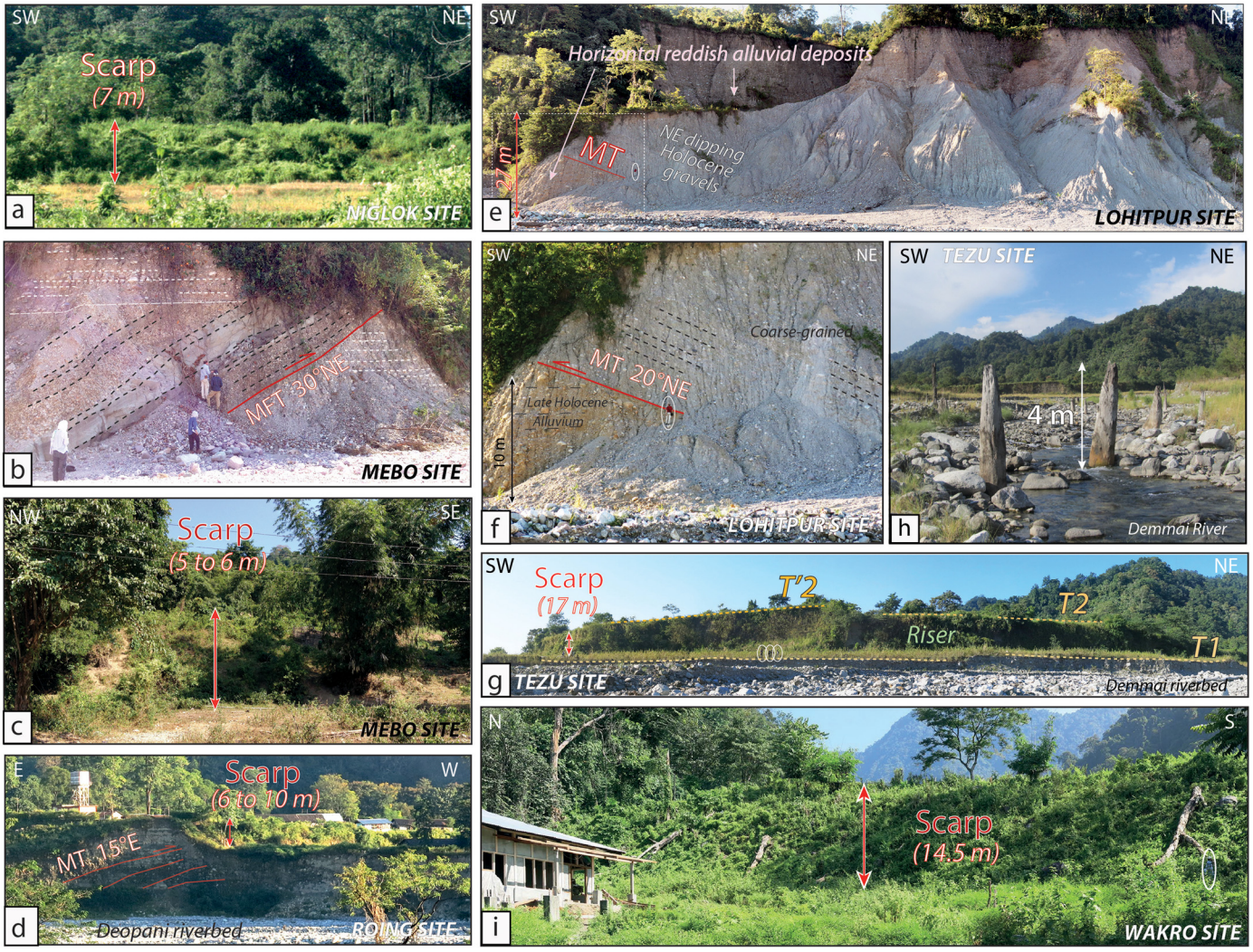

Fig. 4. Morphotectonic markers of active thrusting along the Abor and Mishmi Hills mountain fronts (locations of sites in Fig. 2). (a) Tectonic scarp (about 7 m-high) marking the surface emergence of the MFT along the Abor Hills front, north of Niglok. (b) Section along east bank riser of Siku river, west of Mebo, showing uplifted, flat, modern strath terrace, capping fault-bend folded, Siwalik siltstones/sandstones overthrusted atop flat, modern alluvium by 35°NNE dipping emergent MFT. (c) MFT scarp across young, uplifted Siku terrace just east of rivercut section in Fig. 4b, west of Mebo. (d) Mishmi Thrust scarp (up to 10 m-high and 350 m-long) above rivercut exposing 15°E-dipping MT plane, north of Roing. (e) Rivercut section across 20°NE-dipping Mishmi Thrust along NW bank of Tebang river southwest of Lohitpur. (f) Close-up of Tibang rivercut (Fig. 4e) showing the emergent MT plane emplacing 25°NE-dipping, fine-grained, light grey gravel beds (fault-bend folded) atop sub-horizontal, coarser-grained, buff-colored modern alluvium. That ≈27 m vertically offset young alluvium yields a minimum cumulative thrust slip of ≈79 m (see equation in section 5.2 for more details). (g) Uplifted hanging-wall terraces, NNE of 17 m-high scarp, attesting for cumulative deformation, on Demmai River west bank, east of Tezu. (h) Tree trunks beheaded by 1950 debris flow in Demmai riverbed (Lohit tributary), east of Tezu (cf. Fig. S3). (i) Cumulative, 14 to 15 m-high, MT scarp, southeast of Wakro (Fig. 5C_3).

the elevation difference resulting from the long-term growth of the two ranges (Fig. 3).

3. Geomorphic and stratigraphic evidence for surface thrusting along the Abor and Mishmi range-fronts

We describe here, for the first time along more than 150 km across the Syntaxis, geomorphic and tectonic features attesting to recent, modern, surface thrusting along both the Abor and Mishmi mountain fronts (Note S4, Figs. 2 and 4).

North of Niglok (27.87°N, 95.23°E, Fig. 2), a clear, 6 to 7 m-high and 600 m-long, cumulative tectonic scarp (Fig. 4a), orthogonal to the Sille river cuts across rice paddies. The height of this scarp increases westwards for ≈2 km along the edges of older terraces, and decreases stepwise eastwards to ≈3 m and ≈1.5 m before disappearing towards the river (Fig. S2). As it marks the northern edge of the Assam plain, this scarp clearly corresponds to the frontal emergence of the MFT. Shortly to the east, this thrust steps left northwards by ≈5 km, north of Mikung (27.92°N, 95.24°E, Fig. 2), to bound the uplifted Mirem terraces (Fig. S4). Yet farther northeast, past another ≈2 km northward step, the MFT cuts across Pasighat (28.06°N, 95.32°E, Fig. 2), sharply separating flights of uplifted hanging-wall terraces, initially deposited by the nearly orthogonal Siang-Brahmaputra River, from footwall channels in that river's floodplain (Kali et al., 2012, 2013) (Fig. 6A).

North of Pasighat, past another left-step across the Brahmaputra, the MFT continues northeastwards, bounding uplifted flat surfaces in an area densely covered by forest. In the Siku river valley, west of Mebo (28.17°N, 95.42°E, Fig. 2), a 30° north-dipping thrust fault emplaces similarly dipping beds of mudstones and fractured pebbles atop horizontal layers of coarser cobbles (Fig. 4b). The young-looking, ≈5 m-high surface scarp corresponding to that thrust may be followed along the mountain front for ≈4 km eastwards (Fig. 4b and c). Farther east, the MFT continues northeastwards for about 30 km to the Dibang river outlet (28.29°N, 95.71°E) where it meets almost orthogonally with the MT (Figs. 1 and 2, Note S4).

Between the Dibang and the Deopani rivers (28.16°N, 95.85°E, Fig. 2), the MT runs mostly parallel to the large risers of these two rivers. Just north of Roing, at the Deopani outlet, the thrust veers by 90° to cut the terrace riser along the river's south bank before continuing farther southwards across young terraces of that river for ≈400 m. The north-facing, vertically incised Deopani riser exposes the ≈15° east-dipping MT thrust in section (Fig. 4d). The MT surface trace then continues along the base of an escarpment whose height increases southwards from ≈6 to ≈10 m, bounding the edge of a flat, uplifted alluvial-fan surface. Between Roing and Lohitpur (28.01°N, 96.21°E, Fig. 2), particularly thick, far-reaching debris flows most likely triggered by the 1950 mainshock (Note S5), facing the most prominent landslide scars in the Mishmi Hills, cover the foreland SW of the MT trace. West of Lohitpur, a south-facing rivercut along the Tebang river valley exposes a particularly clear section across the emergent 20°NE-dipping Mishmi Thrust that emplaces sheared, 25°NE dipping Quaternary fluvial gravels on top of younger, horizontally-bedded alluvium (Fig. 4e and f). Farther south, between Tezu (27.92°N, 96.16°E) and Brahmakund (27.87°N, 96.36°E, Fig. 2), the ≈17 m-high MT surface scarp bounds multiple abandoned terraces of the Demmai river, a Lohit tributary (Fig. 4g). Beheaded tree trunks, whose ≈4 m-high tops remain spectacularly incrusted with fluvial pebbles, still stand erect above the present-day Demmai floodplain, attesting to the effect of particularly catastrophic 1950 debris flows, as described by Kingdon-Ward (1953b) (Fig. 4h, S3, and Note S5).

At the Lohit River outlet, the MT bends again southwards, to bound the ≈30 km-long north-south trending mountain front all the way towards the piggy-back side of the northeast dipping limb of the curved, actively growing, Plio-Quaternary Manabhum Anticline (Dasgupta, 2011; Borthakur et al., 2013). Near Wakro (27.78°N, 96.34°E, Fig. 2), both north and south of the Kamlang River, we identified particularly steep and young escarpments and recently uplifted terraces (Figs. 4i and 5). We followed the trace of the MT southwards, northeast of the Manabhum anticline and identified sets of uplifted, abandoned terraces suggesting that recurring thrusting extends along the Upper Dihing Valley possibly as far as Vijaynagar, near the junction of the MT with the northernmost branch of the Sagaing Fault (Figs. 1 and 2, Note S4).

4. Quantitative measurements of 1950 and penultimate thrust offsets

We leveled topographic profiles perpendicular to most of the tectonic scarps we identified to estimate their height and separate recent, potentially 1950 co-seismic throws from older, cumulative ones. We collected quartz-rich samples both atop and inside (depth profiles) the uplifted terraces bounded by such scarps for cosmogenic ^{10}Be dating (technical details in Appendix A4). The results obtained at two key sites on the MT and MFT, as well as the constraints they provide on co-seismic surface deformation, are described in detail below.

At and south of Wakro along the MT, we found three steep scarps, roughly perpendicular to the Kamlang River (Fig. 5). The Mishmi Thrust truncated and uplifted the lowest, most recent, strath terrace (KL, Fig. 5B) by 7.6 ± 0.2 m on the north bank of that river. The strath deposits of this terrace stand upon abraded, exhumed metamorphic bedrock whose top is also uplifted, by 7 ± 0.4 m, relative to the river level downstream from the thrust (Fig. 5C$_1$). Along the hanging wall river-cut edge, the sub-vertical terrace riser is still affected daily by multiple rockslides (Fig. S5A) attesting to ongoing incision. The maximum slope of the convex Kamlang-river thrust scarp is particularly steep (up to 60–70°, Fig. 5C). Such convexity and steepness that are similar to those observed across the co-seismic scarps of contemporary thrust earthquakes (e.g., 2005, $M_w = 7.6$, Muzaffarabad, Pakistan, and of the 1999, $M_w = 7.6$, Chi-Chi, Taiwan, Figs. S6 and S7) suggest that the Kamlang scarp formed during a recent, single event. Two well embedded quartz-rich gneiss boulders sampled on the top of the KL terrace, several meters away from the unstable terrace riser edge, yield ^{10}Be exposure ages of 173 ± 27 yr and 1188 ± 180 yr (AS13-51 and AS13-50, respectively; Fig. 5, Appendix E, and Table S5). These two ages imply rather young terrace abandonment, either a little more than a thousand years ago, or as recently as during the past two centuries. Considering the steep, fresh morphology of the Kamlang scarp, we interpret the youngest cosmogenic age to constrain the onset of floodplain abandonment and therefore the maximum age of co-seismic uplift. In all likelihood, such very recent abandonment should be correlated with the 1950 Assam earthquake, the only known regional event in the entire region large enough to produce the particularly high uplift of the Kamlang terrace. Given the limited number of sample ages discussed here, additional dating is required to corroborate this interpretation.

The other two steep scarps, that bound uplifted alluvial surfaces north and south of the Kamlang River (WK and SK, Fig. 5A), are almost exactly twice as high (≈14.5 and ≈14 m) as the Kamlang terrace scarp, and display composite forms attesting to cumulative uplift (Fig. 5C). The northern scarp shows two slope breaks separating a steep (40°) middle part from an upper bevel and lower colluvium with gentler ≈16° and ≈13° slopes, respectively. The offset of the scarp's steepest central part, most likely due to the last surface rupturing earthquake, is 7.7 ± 0.1 m. This value is essentially identical to the 7.6 ± 0.2 m offset of the youngest KL terrace. The southern scarp also shows distinct slopes upwards (21° and 29°) and downwards (40°) but no symmetry, possibly because of secondary faulting upslope and quarry excavation at the base. Measurements of in situ-produced cosmogenic ^{10}Be concentrations in 7 exposed quartz-rich boulders atop the SK and WK hanging-wall and footwall alluvium are shown in Figs. 5, S8, and Table S5. Two of the three samples from the SK terrace provide consistent exposure ages of 1636 ± 486 yr and 1710 ± 513 yr, yielding a young, mean exposure age of 1670 ± 500 yr. The third sample is ≈1000 yr older (2734 ± 405 yr) and thus may be less representative of the exposure age of the SK terrace (see PDF Fig. S8). On the WK fan surface, the four samples yield exposure ages between 2133 ± 395 and 3292 ± 384 yr, with a mean age of ≈2.8 ± 0.4 kyr. However, a 2 m-deep road cut depth profile across the footwall section of that fan surface yields ^{10}Be concentrations that are best modeled with a 2.3 ± 0.3 kyr age profile (Fig. S8). Within uncertainties, and in view of the different sampling locations, the youngest surface abandonment age (2.1 ± 0.4 kyr) of the Wakro alluvial fan is in fair agreement with that deduced from its depth profile (2.3 ± 0.3 kyr).

Given the aforementioned descriptions, we consider that the youngest ages on both surfaces best constrain exposure ages of ≈2.2 ± 0.5 kyr for the Wakro alluvial fan, and ≈1.7 ± 0.5 kyr for the South Kamlang terrace (WK, SK, respectively on Fig. 5) (Appendix E). The younger age of SK is likely related to its nature and simpler exposure history (emerged river terrace rather than abandoned alluvial fan) and might best constrain the age of surface uplift of both, if contemporary. The simplest scenario accounting for these quantitative observations is a cumulative, ≈14 m co-seismic uplift of the two terraces as a result of two large events, including the 1950 Assam earthquake, with nearly identical vertical throws of ≈7 m. A quantitative analysis of the shapes of these scarps in terms of degradation by diffusion (e.g., Hanks and Wallace, 1985; Tapponnier et al., 1990; Avouac, 1993; Avouac and Peltzer, 1993; Carretier et al., 2002) might be used to corroborate this scenario.

In Pasighat, topographic profiles leveled perpendicular to the MFT scarp across three distinct, uplifted and abandoned Brahmaputra terraces (profile 4 on Fig. 6) constrain the throws due to suc-

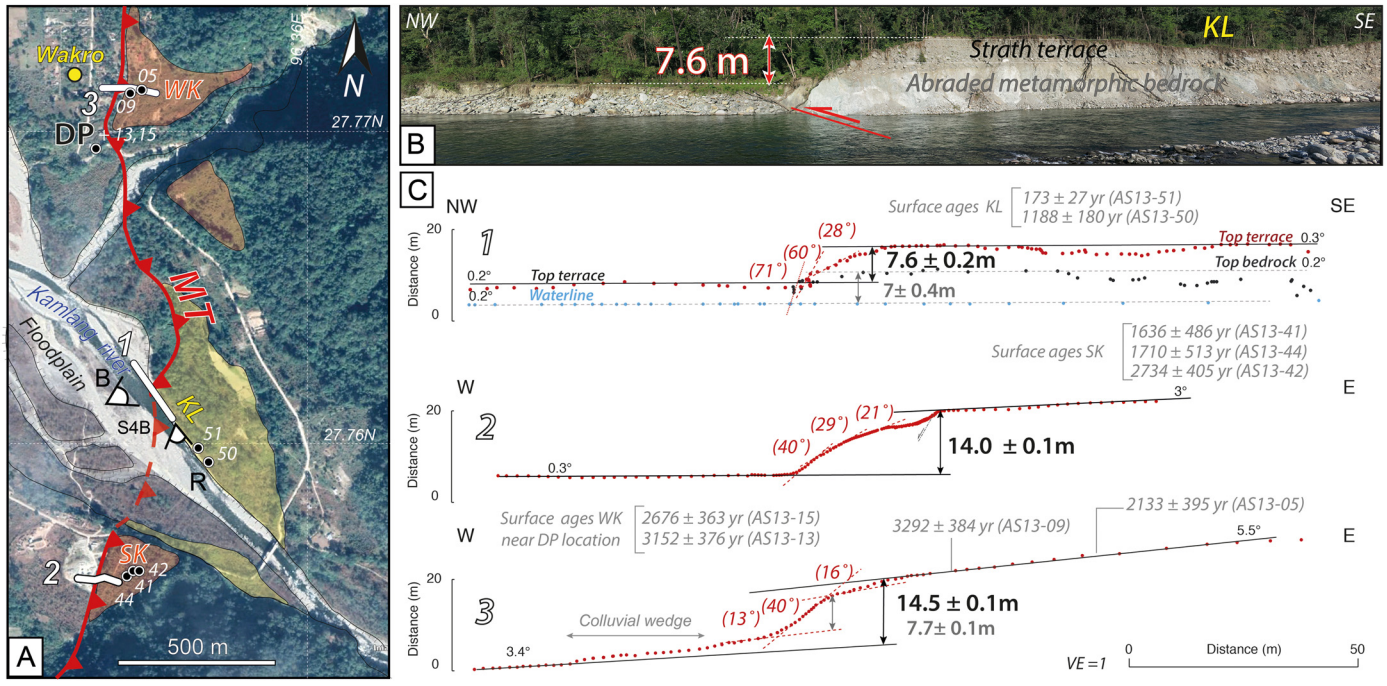

Fig. 5. 1950 surface break along the Mishmi Thrust (MT) near Wakro. A. Map of emergent MT trace (red) and sections across young scarps bounding uplifted alluvial surfaces (yellow and orange). Background image from Google Earth. Numbered white lines correspond to scarp profiles 1, 2, and 3 in Fig. 5C. White point-of-view symbols refer to photographs in Figs. 5B and S5B. Small, numbered black/white circles indicate sample locations (Table S5 and Fig. 5C). R: Rapids. WK: Wakro alluvial fan surface. KL: Kamlang terrace. SK: South Kamlang terrace. B. View of 1950 co-seismic scarp bounding uplifted KL terrace on NE bank of river. C. Topographic profiles 1, 2, and 3 across MT scarps in Fig. 5A.

cessive events. The corresponding seismic scarp heights increase southwestwards from 2.6 ± 0.1 m, to 7.3 ± 0.1 m, and 11.5 ± 0.1 m, across terraces T1, T2, and T3, respectively (Fig. 6). The flat, top and bottom surfaces of the smallest escarpment are offset by a steep, convex upward, up to 56° steep slope that tops a small colluvial wedge (Fig. 6C_1). The two highest scarps have gentler maximum slopes (23° and 29°), with profiles partly smoothed by human action, and larger colluvial wedges (Fig. 6$C_{2,3}$). Even though alteration of the three scarps by road and house construction is evident, we consider the height of the smallest (2.6 ± 0.1 m), steepest, hence youngest, scarp as a minimum bound for the last event throw (Kali et al., 2013; Coudurier-Curveur et al., 2015). A similar, ≈3.1 m-high scarp, studied and trenched ≈400 m northeast of our location, has also been inferred to result from surface faulting in 1950 (Priyanka et al., 2017). The other two scarp heights we measured may be interpreted to yield evidence for cumulative offsets due to one and two comparable earthquakes. In-situ cosmogenic ^{10}Be concentrations derived from 4 samples collected on top of the hanging wall on profile 2 (Terrace T2, Fig. 6$C_{2,4}$) range in age from 2722 ± 290 yr to 4393 ± 432 yr with a mean exposure age of 3.7 ± 1.2 kyr. As in Wakro, the age of the youngest of these samples might be taken to constrain a maximum abandonment age of the T2 terrace and therefore a maximum age for uplift associated with the penultimate event, which would then be younger than 2722 ± 290 yr (Table S5). Here also, however, additional sampling and depth profiling are needed to better constrain the T2 and T3 exposure ages and therefore the earthquake history on the MFT near Pasighat.

5. Solving the 1950 Assam earthquake dilemma?

5.1. Source geometry

5.1.1. A two-fault source model

The combination of relocated aftershocks and landslide scar distributions (Figs. 1–3) strongly suggests that both fault planes ruptured during the 1950 earthquake over a total length of ≈330 km, as strongly supported by field observations of fresh-looking scarps along the Mishmi (MT) and Main Himalayan Frontal (MFT) thrusts (Figs. 4–6). We propose a two-fault source model schematically represented by two planes (orange parallelograms in Fig. 1), whose intersection projects just west of the Dibang valley. They have different widths and dips, consistent with 1/ the lower average elevation of the Abor relative to the Mishmi hills (a factor of ≈2, Figs. 1–3 and S9), 2/ our surface dip measurements (Figs. S10 and S11), and 3/ the depths of the largest 1950, relocated aftershocks (Fig. 3, Table S3). The MT source covers a projected surface area of 180 km by 80 km, from the Myanmar border to the Dibang River (Fig. 1). The MFT source extends over a projected surface area of 150 km by 100 km, from the Dibang to the Subansiri rivers.

The similar orientations of (1) the intersection between both planes, (2) the slip directions in the focal mechanisms, and (3) the average trends of hanging wall GPS vectors relative to India (e.g., Kreemer et al., 2014; Vernant et al., 2014) (Figs. 1, 8, and S12A) suggest similar slip directions on both thrust planes. This would be consistent with oblique slip on each of the thrusts, implying a left-lateral component along the MFT and a right-lateral one along the MT (Fig. S13). Although lateral offsets were generally hard to detect in the field, the respectively left and right stepping geometries of the MFT and MT are in keeping with opposite obliquities of thrusting along both. Alternatively, as suggested by new local GPS data, small scale, clockwise drag-rotation of an Assam micro-block (Gupta et al., 2015), a mechanically reasonable inference at the eastern tip of impinging India, would alleviate the need for a right-lateral slip component along the Mishmi Thrust (Fig. S12B). This, however would still require significant left slip along the MFT. Clearly, more field exploration for kinematic indicators, and higher resolution geodesy are both needed to determine which of the two processes (rotation or oblique slip) is more important.

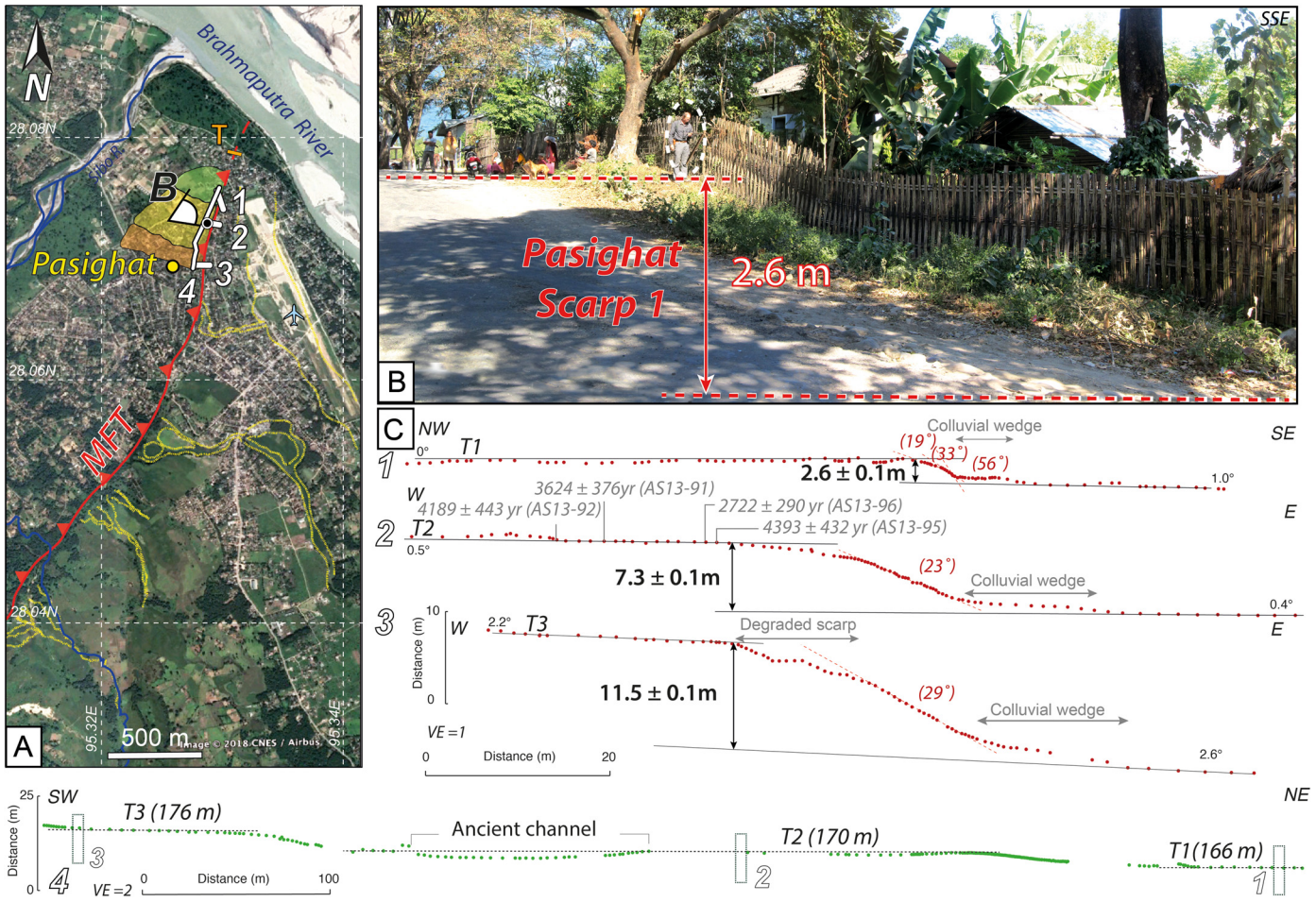

Fig. 6. 1950 surface break along the Main Himalayan Frontal Thrust (MFT) at Pasighat. A. Map of emergent MFT thrust trace and sections across young scarps bounding uplifted Brahmaputra terraces T1, T2, and T3 (green, yellow, and orange surfaces respectively, Fig. 6C). Background image from Google Earth. Numbered white lines correspond to scarp profiles 1, 2, and 3 and terrace surface profile 4 in Fig. 6C. White point-of-view symbol refers to photograph in Fig. 6B. Small, numbered black/white circle indicates samples location (Table S5 and Fig. 6C). Yellow dashed lines indicate beheaded former channels in floodplain. Orange line indicates trench (T) dug by Priyanka et al. (2017). B. View of co-seismic 1950, T1 escarpment modified by road building, north of airport (Profile 1). C. Topographic profiles 1, 2, and 3 across 1950 and cumulative thrust scarp. Profile 4, parallel to scarp, shows elevation differences between terraces T1, T2, and T3.

5.1.2. Crustal and superficial fault dip angles

Considering an ≈30 km-thick seismogenic crust and a downdip slip limit located roughly beneath the high Himalayan range (≈3500 m asl elevation contour, Avouac, 2003; Dhital, 2015), the MT and MFT thrust dip angles would be about 25 and 15°, respectively, in keeping with the ≈28 and ≈14° dips consistent with the aftershocks depth distributions (Fig. 3). The 3D geometry of planes that best fit the relocated aftershock hypocenters and the simplified 3D surface rupture trace may be constrained further using the Petrel E&P software platform (Appendix A3). The resulting MT and MFT planes have dip angles of 25 and 13°, respectively (Figs. 7 and S14). In summary, average dip angles of ≈25–28° for the MT, and ≈13–15° for the MFT, account best for the available geological and geophysical evidence. In keeping with a 25–28° dip for the Mishmi Thrust, the hypocenter depth of the 1950 Assam earthquake would be about 37 ± 3 km (Figs. 3 and 7).

At several sites in the field, our local, detailed mapping and georeferenced profiles also provide strong constraints on the thrusts' shallow dip angles. At Wakro, co-referenced scarp profiles cutting the thrust trace at three different elevations (Fig. 5) constrain a planar, shallow MT dip of 13 ± 1° (3-point method, Appendix A2, Fig. S10 and Table S6). This is less than the 20° measured along the Lohitpur River section (Fig. 4g) but consistent with Himalayan megathrust frontal dips elsewhere (e.g., Malik et al., 2008; Sapkota et al., 2013). At Pasighat, the small elevation difference (≤1.5 m) between 3 co-referenced profiles across the MFT scarps (Fig. S11) makes assessing a dip by using the 3-points method more precarious, but the poorly constrained result (1 ± 0.8°, Appendix A2, and Table S6) may be taken to imply a much shallower dip than those measured along the MT. Note that very shallow MFT surface dips are also visible in trenches at there (Fig. 3a, b in Priyanka et al., 2017) as well as near Niglok (Coudurier-Curveur et al., 2015).

5.2. Shallow and average co-seismic slip amounts

Measured co-seismic vertical throw (u) and thrust dip angle (α) constrain the minimum co-seismic slip: $d = u/\sin(\alpha)$ considering a pure thrusting event with negligible slip obliquity (see section 5.1.1). At Wakro, the 7.6 ± 0.2 m co-seismic throw of the KL terrace and the shallow MT dip of 13 ± 1° would imply, if the young KL exposure age is confirmed, a shallow 1950 down-dip slip of as much as 34 ± 2.5 m. At Pasighat, combining the minimum height (2.6 ± 0.1 m) of the smallest, youngest scarp with a shallow MFT dip of 1 ± 0.8° unfortunately yields an implausibly large 1950 surface down-dip slip (≈150 m!; Appendix A2, Fig. S11, and Table S6), due to the very poor 3-point constraint, clearly not representative of deeper parts of the thrust.

Combining the large scale, constant, average dips compatible with seismic observations (26.5 ± 1.5° and 14 ± 1°) with the

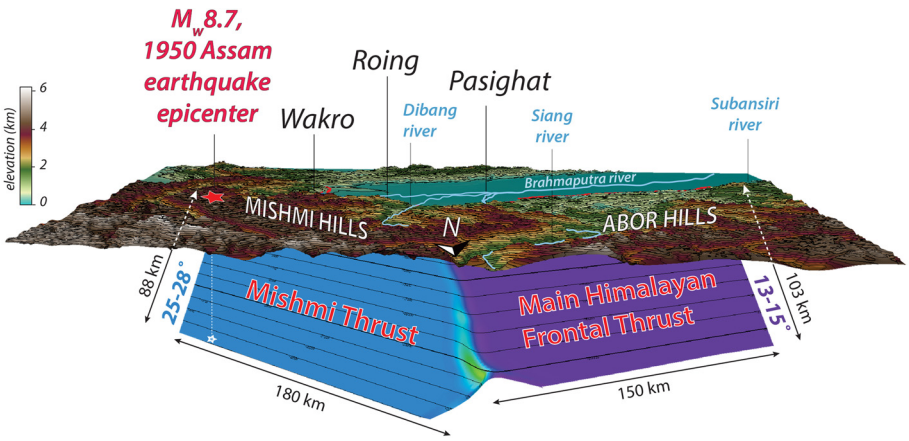

Fig. 7. 3D view of the East Himalayan Syntaxis, with inferred source geometry for the 1950 Assam earthquake. Topography from SRTM3 data. Blue and purple surfaces are reconstructed co-seismic Mishmi Thrust (MT) and Main Himalayan Frontal Thrust (MFT) rupture planes dipping 25–28° and 13–15°, respectively. 3D image was built using Petrel E&P software.

Wakro/Pasighat surface throws (u) of 7.6 ± 0.2 m and 2.6 ± 0.1 m (Figs. 5C_1 and 6C_1) would yield average co-seismic slip values (d) of ≈17 ± 1 m and ≈11 ± 1 m on the MT and MFT, respectively. Note that such slip amounts are compatible with the 16 m average slip calculated by Chen and Molnar (1977) on a unique, low-angle MFT fault.

5.3. Dual first motion focal mechanism

The kinematically complex dual source we propose for the 1950 Assam earthquake likely accounts for the fact that its exact geometry has long been the subject of controversy. Tandon (1955) carried out an early investigation of the focal geometry of the 1950 event, and proposed a normal faulting mechanism with parameters inferred to be $\phi = 270°$; $\delta = 75°$; $\lambda = 285°$ (Fig. 8A and Table 1). As later discussed by Ben-Menahem et al. (1974), however, several of his readings might have been erroneous, and his methodology, which predated the introduction of the double-couple concept, also did not handle core phases, the latter being incompatible with normal faulting. His dataset remains valuable, however, notably for stations in Central and Southern India. Ben-Menahem et al. (1974) investigated the focal mechanism of the 1950 earthquake based on the interpretation of both first motions and spectral amplitudes of long-period surface waves. They proposed a strike-slip solution on a steeply dipping plane ($\phi = 334°$, $\delta = 60°$, $\lambda = 175°$; Fig. 8B and Table 1) that would correspond roughly to the Jiali-Po-Qu-Lohit fault, later identified as a large, active, strike-slip fault (e.g., Molnar and Tapponnier, 1975; Tapponnier and Molnar, 1977; Ni and York, 1978; Armijo et al., 1989). Subsequently, Chen and Molnar (1977) argued that a shallow dipping thrust with a strike close to that of the MFT ($\phi = 260°$, $\delta = 12°$, $\lambda = 90°$) (Fig. 8C and Table 1) provided an equally acceptable fit to the first motion dataset. In fact, neither the steep dip of the Po-Qu-Lohit fault, nor the length of an inferred rupture along it can account for the distribution of aftershocks and magnitude of the 1950 event (e.g., Armijo et al., 1989). Furthermore, while Ben-Menahem et al.'s (1974) solution skillfully runs fault planes through available first motion datasets (assuming a crustal source velocity of 6.5 km/s, and ignoring most of Tandon's (1955) data from stations in India), it remains unconvincing given impulsive arrivals in the vicinity of its proposed null axis. On the other hand, while Chen and Molnar's (1977) pure thrust solution fits well with the broad aftershock zone beneath the eastern Himalayas and with the MFT's ≈NE-SW trend and dip consistent with our field observations, it accounts neither for the epicenter location in the Mishmi Hills nor for the dominant 1950 thrusting and landslides along the nearly orthogonal MT. It seems clear that a composite source, as suggested by our field results and the broader aftershock/landslide distribution, with a possible time lag of a few seconds between ruptures on two thrust faults, is required.

We thus re-assessed the first motion dataset by personally reading records at 12 historical stations (all compressional except Jakarta), and complementing it by first motions reported by the ISS and by Tandon (1955) (Fig. 8). We find that the fault geometry derived from our field investigation along the MFT ($\phi = 245°$, $\delta = 15°$, $\lambda = 70°$) is compatible with the first-arrival dataset on Fig. 8D, while a source on the MT ($\phi = 315°$, $\delta = 20°$, $\lambda = 120°$) would violate the dilatational arrivals at Brisbane and Riverview, in Eastern Australia (Fig. 8E). Such observations might be compatible with an initial rupture on the MFT, and a time-lagging rupture on the MT not contributing to first motion polarities. However, this interpretation would be at odds with the mutually consistent locations of the 1950 epicenter 80 km NE of the Mishmi Thrust (Figs. 1–2; Tandon, 1955; Ben-Menahem et al., 1974; Chen and Molnar, 1977). Hence, the 1950 rupture must have nucleated on the MT, whose plane, with an average dip of 20° (Fig. 8E), would fit the entire dataset save for arrivals at Brisbane and Riverview, whose picks we unfortunately could not independently confirm. Additionally, 3 dilatational arrivals (at Cartuja, Owase, and Nagasaki), which are inside the densest, best-defined compressional cluster, are in all likelihood erroneous. To accommodate deep aftershocks, structural geology, field observations, and possible changes of dip at depth, we consider an average dip of 25° for the source on the MT that best fits the entire dataset. The two sub-mechanisms ($\phi = 315°$, $\delta = 25°$, $\lambda = 120°$, and $\phi = 245°$, $\delta = 15°$, $\lambda = 70°$, on the MT and MFT, respectively), with scalar ratios of 1:1.6 (see potency ratios, below), combine into a nearly pure double-couple oriented $\phi = 293°$, $\delta = 16°$, $\lambda = 107°$ (Fig. 8 and Table 1).

Remarkably, the full, combined, 5-dimensional moment tensor derived from the dual (MT+MFT) source model we propose (Fig. 8) satisfies all clearly non-erroneous first motion arrivals, including Brisbane and Riverview (Fig. S15). This excellent fit, however, still runs into the problem that the source could not have been instantaneous, given the necessary propagation time (on order of tens of seconds) over a distance of at least 100 km between the two rupture segments.

5.4. Independent seismic moment estimates

5.4.1. Seismic moment from field observations

Under the assumption of uniform slip on the faults, we can estimate the resulting seismic potencies P_o of both fault planes corresponding to the product of the average slip d and the ruptured area S. Using $d = 17$ m and 11 m, and $S = 16\,000$ km^2

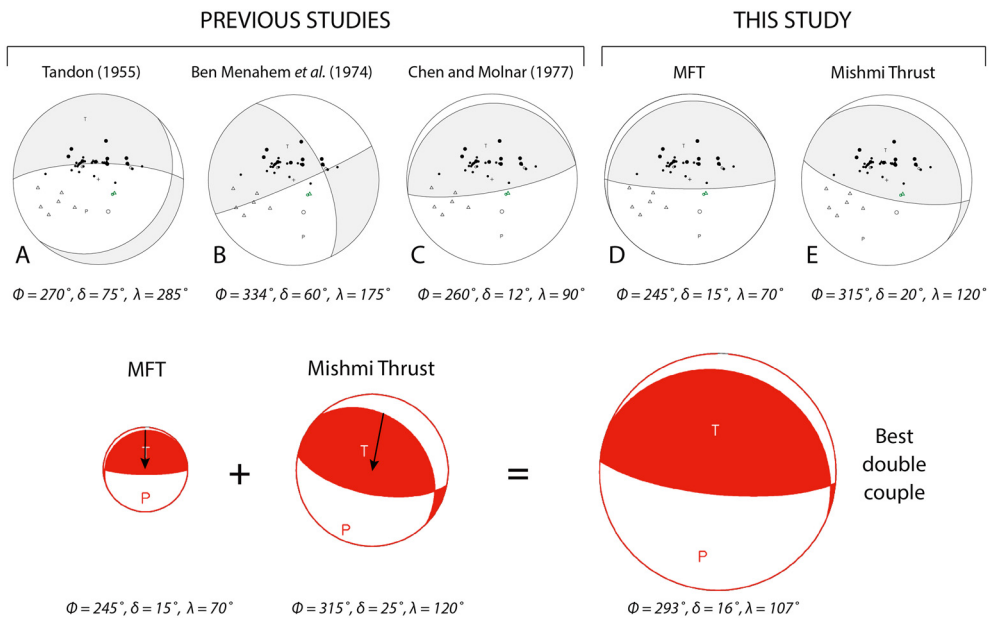

Fig. 8. (Top) First-motion focal mechanisms for the 1950 Assam earthquake. The dataset used combines polarities read as part of this study (large dots), and reported from the ISS (small dots), or transcribed from Tandon (1955) (small triangles, all Indian stations). Solid and open symbols are compressional and dilatational arrivals, respectively. A. Normal faulting mechanism proposed by Tandon (1955): note inconsistencies for large distances. B. Strike-slip mechanism from Ben-Menahem et al. (1974): note inconsistencies for several Indian stations. C. Shallow-dipping thrust faulting solution from Chen and Molnar (1977): note remaining inconsistencies at a few of Tandon's (1955) Indian stations. D. Mechanism for shallow-dipping thrusting on MFT: note superior fit to entire first motion dataset. E. Mechanism for oblique thrusting on MT: note only small near nodal inconsistencies at 2 Australian stations. (Bottom) Focal mechanisms combination consistent with field observations. (Left) Mechanisms on MFT and MT, respectively, with beachballs scaled linearly to seismic moments. Black arrows are slip vectors. (Right) Best double-couple derived from combined MFT+MT solutions.

and 15 500 km^2 (Fig. 7), yields potencies of ≈270 and ≈170 km^3 for the MT and MFT fault planes, respectively. Assuming a crustal rigidity μ of 3×10^{10} Pa (or N/m^2), the corresponding seismic moments ($M_0 = \mu P_0$) would be $\approx 8 \times 10^{21}$ and $\approx 5 \times 10^{21}$ N·m, on the MT and MFT, respectively. This would imply a moment sum of 1.3×10^{22} N·m corresponding to a moment magnitude of $M_w = 8.7$ (Table 1).

Taking more gentle dips for the thrusts, consistent with our field measurements, would increase the resulting slips on the MFT and MT to ≈20 and ≈40 m, respectively, and the resulting moment sum to 2.8×10^{22} N·m ($M_w = 8.9$). Such larger values, however, should only be considered as upper limits since, as inferred for recent megathrust earthquakes (e.g., 2011 Tohoku event; Ammon et al., 2011; Lee et al., 2011), one might expect spatial slip heterogeneities on the thrusts, such as slip decrease and/or dip increase with increasing depth.

5.4.2. Seismic moment from mantle waves

Based on our best double-couple geometry, we computed the spectral amplitudes of mantle Rayleigh and Love waves (Okal and Talandier, 1989) from long-period records at Uppsala, Göttingen, San Juan, and Huancayo, complemented by our previous dataset at Pasadena (Okal, 1992). Such amplitudes require a seismic moment of $\approx 1.0 \times 10^{22}$ N·m at the longest resolvable periods (200–250 s; Fig. 9). This value is compatible with, although 23% smaller than, that estimated from our field observations. The discrepancy may be attributed to uncertainties on the depth extent of faulting and to probable slip heterogeneities on the fault planes. On the other hand, the inferred total potency would amount to ≈440 km^3, a factor of 1.6 smaller than suggested by Ben-Menahem et al. (1974). Our moment is also compatible with Chen and Molnar's (1977) estimate (9.5×10^{21} N·m) computed for a low angle thrust on the MFT only (Table 1). To our knowledge, such moment values still single out the 1950 Assam earthquake as the only continental earthquake on record with a seismic moment value of 10^{22} N·m ($M_w = 8.6/8.7$). Finally, the weak dependence of M_c on frequency (slope of only −0.06 logarithmic units per mHz, Fig. 9) indicates that, despite its composite mechanism, the 1950 Assam earthquake did not display anomalous source slowness (generally associated with slopes of −0.08 or more in absolute value) (e.g., Okal and Borrero, 2011; Okal, 2013). Rather, this slope suggests a rupture time of no more than ≈65 s, a standard value for the proposed dimensions of the composite rupture.

5.5. Return time

The cosmogenic ages of the cumulative, 14 m offset terrace doublets near Wakro suspected to have recorded near-identical uplift amounts by two successive events, including the 1950 earthquake, may be used to estimate the return time of such events. The older ages (2.3 ± 0.3 kyr, 2.1 ± 0.4 yr, and 1.7 ± 0.5 yr; Fig. S8, Section 4) on terraces WK and SK, north and south of the Kamlang River, respectively, imply nearly identical uplift by a comparably great event at least 1200 and possibly as much as 2600 yr earlier (i.e., 1900 ± 700 yr). Following the same logic at Pasighat, the less well constrained youngest abandonment age of the second terrace (T2, Fig. 6), which likely recorded uplift by 2 events, would suggest a maximum return time of ≈2700 yr between these events. Such return interval on the Main Himalayan Frontal Thrust would nevertheless be compatible with the upper bound of that estimated at Wakro along the Mishmi Thrust.

Local, recently published interseismic GPS velocities imply a shortening rate of 17 ± 0.5 mm/yr across the MT (e.g., Devachandra et al., 2014; Gupta et al., 2015). That shortening rate and the minimum 34 ± 2.5 m 1950 co-seismic slip we infer at Wakro, would be consistent with a return time of ≈1980 ± 160 yr for 1950 Assam-size events on the MT. Such recurrence interval would be compatible with that (≈1900 ± 700 yr) derived from cosmogenic dating of uplifted terraces at the same location. It is clear however that more quantitative geomorphic and age constraints along both thrusts are needed to better assess the recurrence interval of great, 1950-type earthquakes across the East Himalayan Syntaxis.

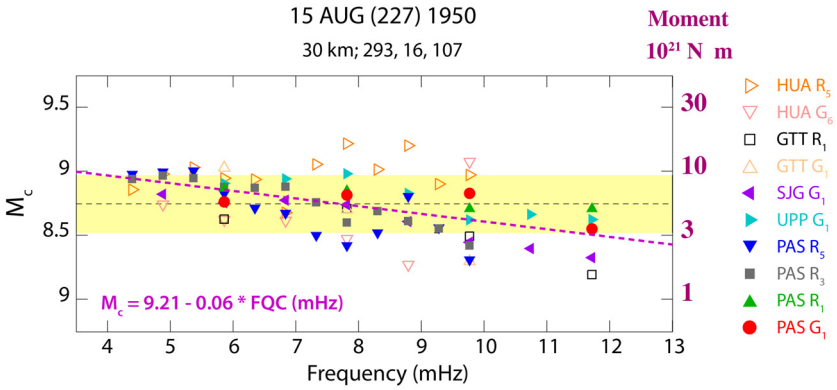

Fig. 9. Determination of seismic moment from mantle Rayleigh and Love waves. Colored symbols show corrected mantle magnitude M_c (Okal and Talandier, 1989), based on Fig. 8 composite MFT+MT focal mechanism, at various stations (HUA, GTT, SJC, UPP, and PAS are Huancayo, Göttingen, San Juan, Uppsala, and Pasadena, respectively; R_i and G_i are subsequent surface wave passages). Dashed violet line shows best linear fit to M_c values as a function of frequency (bottom left equation). Black dashed line and yellow band show averaged M_c value and associated standard deviation, respectively, across entire frequency spectrum. Weak moment increase with period suggests a value of 1×10^{22} N·m at the longest available periods (~250 s).

6. Conclusions

Even though the exact geometry of the seismic source of the great 1950 Assam earthquake remains to be better ascertained, our wide-ranging, multi-method observations and measurements support the co-involvement of two distinct, nearly orthogonal thrust planes. The earthquake appears to have been associated with sub-parallel components of oblique slip both on the shallow-dipping part of Himalaya's Main Frontal Thrust, beneath the Siang window, and on the significantly steeper Mishmi Thrust. Such a dual fault geometry and the correlated amounts of slip on both thrusts are compatible with a composite mainshock focal mechanism and with a total seismic moment of 1.3×10^{22} N·m that confirms it as the largest continental event ever quantified. Our landslide scar and relocated aftershock distributions constrain the extent of the rupture area, ≈330 km by 90 km, across the East Himalayan Syntaxis. Our field measurements likely attest to a minimum ≈200 km-long primary 1950 surface rupture along the Mishmi and Abor hills fronts. The fact that the ratios between the co-seismic surface throws on the MFT and MT, and between the two mountain frontal elevations are comparable (0.34 and 0.44, respectively; Figs. 3 and S9) is in keeping with such a complex, dual source and highlights their strong link with long-term topographic growth (e.g., King et al., 1988). We interpret our 3D thrust-dip measurement (≈ 13°) near Wakro to indicate that the 1950 shallow seismic slip on the Mishmi Thrust there reached at least 34 ± 2.5 m, given the 7.6 ± 0.2 m seismic uplift of the young Kamlang River terrace. In the same area, older, twice larger, cumulative terrace uplifts of 14 and 14.5 m may be taken to imply near-characteristic slip behavior during two similar great earthquakes. The GPS shortening rate and our cosmogenic ^{10}Be terrace ages are consistent with a first-order, nearly bi-millennial return time for such mega-quakes. The very large amounts of co-seismic slip and uplift on the Mishmi Thrust (>30 and >7 m, respectively), where the thrust cuts the youngest deposits at the level of a permanent river channel, rule out the use of classic paleoseismological techniques to investigate the long-term history and return times of Thrust Mega-quakes ($M \geq 8$), except at atypical, possibly unreliable sites. Our findings around the Assam cusp provide further evidence that large Himalayan megathrust earthquakes are not "blind", supporting mechanical models in which the bulk of the GPS-measured, elastic shortening across the large mountain range is ultimately and primarily released by slip on the frontal, emergent thrusts.

Acknowledgements

This research is partly supported by the National Research Foundation Singapore and the Singapore Ministry of Education under the Research Centres of Excellence initiative in the framework of an MoU with the CSIR-North East Institute of Science and Technology (Jorhat, India) co-signed by P. Banerjee, P. Tapponnier, and S. Baruah, with contribution from IPG Strasbourg (France). We thank S. R. Ildefonso (Aero 360 Solutions, Philippines), S. Sharma and S. Baruah (NEIST, India), and A. Ahsan (Geological Survey of Bangladesh) for their essential contribution in the field (topographic surveys, rock sampling). We thank Laurent Bollinger (CEA, France) for the tri-stereo Pleiades image correlation at Pasighat. Pleiades DEMs were processed using CNES data (2014), Astrium Services Distribution/ Spot Image S.A., France (all rights reserved, commercial use forbidden). We acknowledge help from Ota Kulhánek and Don Helmberger to access the Uppsala and Pasadena seismological archives. We thank the ASTER AMS national facility (CEREGE, Aix-en-Provence, France, supported by INSU-CNRS, IRD, and CEA) and Dr. Steven Binnie (AMS Cologne, Germany) for cosmogenic dating. PT also thanks Prof. A. Kausar (Geological survey of Pakistan) for his contribution in the field near Muzaffarabad, Azad-Kashmir, in January 2006. P. Tapponnier is grateful to the Asian School of the Environment (ASE) for allowing him to complete this work by extending his contract at NTU for one year and a half. We are grateful to the Editor and three anonymous reviewers for fastidious and constructive comments that helped improve the original manuscript.

This work comprises Earth Observatory of Singapore contribution no. 269.

Appendix. Supplementary material

Supplementary material related to this article can be found online at https://doi.org/10.1016/j.epsl.2019.115928. These data include the Google map of the most important areas described in this article.

References

Abe, K., 1981. Magnitudes of large shallow earthquakes from 1904 to 1980. Phys. Earth Planet. Inter. 27, 72–92. https://doi.org/10.1016/0031-9201(81)90088-1.

Ader, T., et al., 2012. Convergence rate across the Nepal Himalaya and interseismic coupling on the Main Himalayan Thrust: implications for seismic hazard. J. Geophys. Res. 117, B04403. https://doi.org/10.1029/2011JB009071.

Ammon, C.J., Lay, T., Kanamori, H., Cleveland, M., 2011. A rupture model of the 2011 off the Pacific coast of Tohoku earthquake. Earth Planets Space 63, 693–696. https://doi.org/10.5047/eps.2011.05.015.

Armijo, R., Tapponnier, P., Han, T., 1989. Late Cenozoic right-lateral strike slip faulting in Southern Tibet. J. Geophys. Res. 94 (B3), 2787–2838. https://doi.org/10.1029/JB094iB03p02787.

Avouac, J.-P., 1993. Analysis of scarp profiles: evaluation of errors in morphologic dating. J. Geophys. Res. 98 (B4), 6745–6754. https://doi.org/10.1029/92JB01962.

Avouac, J.-P., Peltzer, G., 1993. Active tectonics in southern Xinxiang, China: analysis of terrace riser and normal fault scarp degradation along the Hotan-Qira fault system. J. Geophys. Res. 98, 21773–21807. https://doi.org/10.1029/93JB02172.

Avouac, J.-P., 2003. Mountain building, erosion, and the seismic cycle in the Nepal Himalaya. Adv. Geophys. 46, 1–80. https://doi.org/10.1016/S0065-2687(03)46001-9.

Ben-Menahem, A., Aboodi, E., Schild, R., 1974. The source of the great Assam earthquake: an interplate wedge motion. Phys. Earth Planet. Inter. 9, 265–289. https://doi.org/10.1016/0031-9201(74)90056-9.

Bollinger, L., et al., 2004. Stress buildup in the Himalaya. J. Geophys. Res. 109 (B11405). https://doi.org/10.1029/2003JB002911.

Bollinger, L., et al., 2014. Estimating the return times of great Himalayan earthquakes in eastern Nepal: evidence from the Patu and Bardibas strands of the Main Frontal Thrust. J. Geophys. Res., Solid Earth 119, 7123–7163. https://doi.org/10.1002/2014JB010970.

Borthakur, A.N., et al., 2013. Challenges for future prospects in foreland thrust belt area – a case study from Manabhum, NE India. Presented at the 10th Biennal International Conference & Exposition.

Carretier, S., Ritz, J.F., Jackson, J., Bayasgalan, A., 2002. Morphological dating of cumulative reverse fault scarps: examples from the Gurvan Bogd fault system, Mongolia. Geophys. J. Int. 148 (2), 256–277. https://doi.org/10.1046/j.1365-246X.2002.01007.x.

Chen, W.P., Molnar, P., 1977. Seismic moments of major earthquakes and the average rate of slip in central Asia. J. Geophys. Res. 82 (20), 2945–2969. https://doi.org/10.1029/JB082i020p02945.

Coudurier-Curveur, A., et al., 2014a. Primary surface rupture of the 1950 Assam earthquake. Presented at the Asia Oceania Geosciences Society Meeting. Sapporo, Japan. Abstract.

Coudurier-Curveur, A., et al., 2014b. Active tectonic uplift in the eastern Himalayan syntaxis: geomorphic traces of the 1950 Assam earthquake rupture. Presented at the Himalaya Karakorum Tibet Workshop. Kathmandu, Nepal. Abstract.

Coudurier-Curveur, A., et al., 2015. Surface Break and Coseismic Slip of the Great 1950 Assam Earthquake and Previous Events along the Eastern Himalayan Syntaxis. Presented at the American Geophysical Union, Fall Meeting, San Francisco, USA. Abstract #T31A-2842.

Dasgupta, S., 2011. Earthquake geology, geomorphology and hazard scenario in northeast India: an appraisal. Presented at the National Workshop on Earthquake Risk Mitigation Strategy in North East AASC-NIDM, Guwahati, Assam, India, pp. 24–39.

Devachandra, M., Kundu, B., Catherine, J., Kumar, A., Gahalaut, V.K., 2014. Global Positioning System (GPS) measurements of crustal deformation across the frontal Eastern Himalayan Syntaxis and seismic-hazard assessment. Bull. Seismol. Soc. Am. 104 (3), 1518–1524. https://doi.org/10.1785/0120130290.

dePolo, C.M., Slemmons, D.B., 1990. Estimation of earthquake size for seismic hazards. In: Krinitzsky, E.L., Slemmons, D.B. (Eds.), Neotectonics in Earthquake Evaluation. In: Geological Society of America Reviews in Engineering Geology, vol. 8. Boulder, Colorado.

Dhital, M.R., 2015. Geology of the Nepal Himalaya: regional perspective of the classic collided orogen. Reg. Geol. Rev. https://doi.org/10.1007/978-3-319-02496-7.

Gupta, T.D., et al., 2015. Kinematics and strain rates of the Eastern Himalayan Syntaxis from new GPS campaigns in Northeast India. Tectonophysics 655, 15–26. https://doi.org/10.1016/j.tecto.2015.04.017.

Gutenberg, B., Richter, C.F., 1954. Seismicity of the Earth and Associated Phenomena. Princeton Univ. Press. 310 pp.

Hanks, T.C., Wallace, R.E., 1985. Morphological analysis of the Lake Lahontan shoreline and Beachfront fault scarps, Pershing County, Nevada. Bull. Seismol. Soc. Am. 75 (3), 835–846.

Herrin, E., Taggart, J., Brown, C.F., 1962. Machine computation 201 of earthquake hypocenters. J. Grad. Res. Center 30, 79–106.

Jayangondaperumal, R., Wesnousky, S., Choudhuri, K., 2011. Near-surface expression of Early to late Holocene displacement along the Northeastern Himalayan Frontal Thrust at Marbang Korong Creek, Arunachal Pradesh, India. Bull. Seismol. Soc. Am. 101 (6), 3060–3064. https://doi.org/10.1785/0120110051.

Kali, E., et al., 2012. Tectonic geomorphology and active megathrust traces in the East-Himalayan Syntaxis. Presented at the Himalayan Karakorum Tibet Workshop.

Kali, E., et al., 2013. Tectonic geomorphology, aftershock relocation, and sources of the great 1950 and 1897 East Himalayan earthquakes. Presented at the American Geophysical Union, Fall Meeting 2013. Abstract T43A-2643.

Kanamori, H., Allen, C.R., 1986. Earthquake repeat time and average stress drop. In: Das, S., Boatwright, J., Scholz, C.H. (Eds.), Earthquake Source Mechanics.

Keefer, D.K., 1994. The importance of earthquake-induced landslides to long term slope erosion and slope-failure hazards in seismically active regions. Geomorphology 10 (1), 265–284. https://doi.org/10.1016/0169-555X(94)90021-3.

King, G.C.P., Stein, R.S., Rundle, J.B., 1988. The growth of geological structures by repeated earthquakes. 1. Conceptual framework. J. Geophys. Res. 93 (B11), 13,307–13,318. https://doi.org/10.1029/JB093iB11p13307.

Kingdon-Ward, F., 1951. Notes on the Assam earthquake. Nature 167, 130–131. https://doi.org/10.1038/167130a0.

Kingdon-Ward, F., 1953a. The earthquake. Wide World Mag., 380–384.

Kingdon-Ward, F., 1953b. The Assam earthquake of 1950. Geogr. J. 119 (2), 169–182. https://doi.org/10.2307/1791200.

Kreemer, C., Blewitt, G., Klein, E.C., 2014. A geodetic plate motion and Global Strain Rate Model. Geochem. Geophys. Geosyst. 15, 3849–3889. https://doi.org/10.1002/2014GC005407.

Kumar, S., et al., 2001. Earthquake recurrence and rupture dynamics of Himalayan Frontal Thrust, India. Science 294 (5550), 2328–2331. https://doi.org/10.1126/science.1066195.

Kumar, S., et al., 2010. Paleoseismological evidence of surface faulting along the northeastern Himalayan front, India: timing, size, and spatial extent of great earthquakes. J. Geophys. Res. 115, B12422. https://doi.org/10.1029/2009JB006789.

Lee, S.-J., Huang, B.-S., Ando, M., Chiu, H.-C., Wang, J.-H., 2011. Evidence of large scale repeating slip during the 2011 Tohoku-Oki earthquake. Geophys. Res. Lett. 38, L19306. https://doi.org/10.1029/2011GL049580.

Malik, J.N., Nakata, T., Philip, G., Suresh, N., Virdi, N.S., 2008. Active fault and paleoseismic investigation: evidence of a historic earthquake along Chandigarh Fault in the Frontal Himalayan zone, NW India. Himal. Geol. 29 (2), 109–117.

Meunier, P., Hovius, N., Haines, J.A., 2007. Regional pattern of earthquake-triggered landslides and their relation to ground motion. Geophys. Res. Lett. 34, L20408. https://doi.org/10.1029/2007GL031337.

Molnar, P., Deng, Q., 1984. Faulting associated with large earthquakes and the average rate of deformation in Central and Eastern Asia. J. Geophys. Res. 89 (B7), 6203–6227. https://doi.org/10.1029/JB089iB07p06203.

Molnar, P., Tapponnier, P., 1975. Cenozoic tectonics of Asia: effects of a continental collision. Science 189 (4201), 419–426. https://doi.org/10.1126/science.189.4201.419.

Nakata, T., 1989. Active faults of the Himalaya of India and Nepal. Spec. Pap., Geol. Soc. Am. 232, 243–264. https://doi.org/10.1130/SPE232-p243.

Ni, J., York, J.E., 1978. Late Cenozoic tectonics of the Tibetan Plateau. J. Geophys. Res. 83 (B11), 5377–5384. https://doi.org/10.1029/JB083iB11p05377.

Nilsen, T.H., Brabb, E.E., 1975. Landslides. In: Borcherdt, R.D. (Ed.), Studies for Seismic Zonation of the San Francisco Bay Region. U.S. Geol. Survey Prof. Paper 941-A, pp. A75–A87.

Okal, E.A., 1992. Use of the mantle magnitude M_m for the reassessment of the seismic moment of historical earthquakes. I: shallow events. Pure Appl. Geophys. 139, 17–57. https://doi.org/10.1007/BF00876825.

Okal, E.A., 2013. From 3-Hz P waves to ${}_0S_2$: no evidence of a slow component to the source of the 2011 Tohoku earthquake. Pure Appl. Geophys. 170, 963–973. https://doi.org/10.1007/s00024-012-0500-x.

Okal, E.A., Borrero, J.C., 2011. The "tsunami earthquake" of 22 June 1932 in Manzanillo, Mexico: seismological study and tsunami simulations. Geophys. J. Int. 187, 1443–1459. https://doi.org/10.1111/j.1365-246X.2011.05199.x.

Okal, E.A., Talandier, J., 1989. M_m: a variable period mantle magnitude. J. Geophys. Res. 94, 4169–4193. https://doi.org/10.1029/JB094iB04p04169.

Poddar, M.C., 1950. The Assam earthquake of 15th August 1950. Indian Miner. 4, 167–176.

Priyanka, R.S., et al., 2017. Primary surface rupture of the 1950 Tibet-Assam great earthquake along the eastern Himalayan front, India. Sci. Rep. 7 (5433). https://doi.org/10.1038/s41598-017-05644-y.

Rajendran, K., Rajendran, C.P., 2011. Revisiting the earthquake sources in the Himalaya: perspective on past seismicity. Tectonophysics 504, 75–88. https://doi.org/10.1016/j.tecto.2011.03.001.

Ramachandra Rao, M.B., 1953. A compilation of papers on the Assam earthquake of August 15, 1950. Cent. Board Geophys. 1.

Reddy, D.V., et al., 2009. The great 1950 Assam earthquake revisited: field evidences of liquefaction and search for paleoseismic events. Tectonophysics 474, 463–472. https://doi.org/10.1016/j.tecto.2009.04.024.

Rees, B.A., Okal, E.A., 1987. The depth of the deepest historical earthquakes. Pure Appl. Geophys. 125, 699–715. https://doi.org/10.1007/BF00878029.

Sapkota, S.N., et al., 2013. Primary surface ruptures of the great Himalayan earthquakes in 1934 and 1255. Nat. Geosci. 6, 71–76. https://doi.org/10.1038/ngeo1669.

Tandon, A.N., 1950. The very great earthquake of August 15, 1950. Sci. Cult. 16 (4).

Tandon, A.N., 1954. Study of the great Assam earthquake of August 1950 and its aftershocks. Indian J. Meteorol. Geophys. 5, 95–137.

Tandon, A.N., 1955. Direction of faulting in the Great Assam Earthquake of 15 August 1950. Indian J. Meteorol. Geophys. 6, 61–64.

Tapponnier, P., Molnar, P., 1977. Active faulting and tectonics in China. J. Geophys. Res. 82 (20), 2905–2930. https://doi.org/10.1029/JB082i020p02905.

Tapponnier, P., et al., 1990. Active thrusting and folding in the Qilian Shan, and decoupling between upper crust and mantle in northeastern Tibet. Earth Planet. Sci. Lett. 97, 382–403. https://doi.org/10.1016/0012-821X(90)90053-Z.

Vernant, P., et al., 2014. Clockwise rotation of the Brahmaputra Valley relative to India: tectonic convergence in the Eastern Himalaya, Naga Hills, and Shillong Plateau. J. Geophys. Res., Solid Earth 119, 6558–6571. https://doi.org/10.1002/2014JB011196.

Wells, D.L., Coppersmith, K.J., 1994. New empirical relationships among magnitude, rupture length, rupture width, rupture area, and surface displacement. Bull. Seismol. Soc. Am. 84 (4), 974–1002.

Wysession, M.E., Okal, E.A., Miller, K.L., 1991. Intraplate seismicity of the Pacific Basin, 1913–1988. Pure Appl. Geophys. 135, 261–359. https://doi.org/10.1007/BF00880241.

Yeats, R.S., et al., 1992. The Himalayan frontal fault system. Ann. Tecton. VI, 85–98. Special Issue, Complement.

Yuan, R.M., et al., 2013. Density distribution of landslides triggered by the 2008 Wenchuan earthquake and their relationships to peak ground acceleration. Bull. Seismol. Soc. Am. 103 (4), 2344–2355. https://doi.org/10.1785/0120110233.